9618 *Biochemistry* **2009,** *48,* 9618–9626
DOI: 10.1021/bi9012484

BIOCHEMISTRY
including biophysical chemistry & molecular biology
Article

Structural and Metabolic Specificity of Methylthiocoformycin for Malarial Adenosine Deaminases[†,‡]

Meng-Chiao Ho,[§,@] María B. Cassera,[§,@] Dennis C. Madrid,[∥] Li-Min Ting,[∥,⊥] Peter C. Tyler,[#] Kami Kim,[∥,⊥] Steven C. Almo,[§] and Vern L. Schramm*[,§]

[§]*Department of Biochemistry and* [∥]*Department of Microbiology and Immunology and* [⊥]*Department of Medicine, Albert Einstein College of Medicine, Yeshiva University, Bronx, New York 10461, and* [#]*Carbohydrate Chemistry Group, Industrial Research Ltd., Lower Hutt, New Zealand* [@]*These authors contributed equally to this study.*

Received July 21, 2009; Revised Manuscript Received August 30, 2009

ABSTRACT: *Plasmodium falciparum* is a purine auxotroph requiring hypoxanthine as a key metabolic precursor. Erythrocyte adenine nucleotides are the source of the purine precursors, making adenosine deaminase (ADA) a key enzyme in the pathway of hypoxanthine formation. Methylthioadenosine (MTA) is a substrate for most malarial ADAs, but not for human ADA. The catalytic site specificity of malarial ADAs permits methylthiocoformycin (MT-coformycin) to act as a *Plasmodium*-specific transition state analogue with low affinity for human ADA [Tyler, P. C., Taylor, E. A., Fröhlich, R. G. G., and Schramm, V. L. (2007) *J. Am. Chem. Soc. 129*, 6872−6879]. The structural basis for MTA and MT-coformycin specificity in malarial ADAs is the subject of speculation [Larson, E. T., et al. (2008) *J. Mol. Biol. 381*, 975−988]. Here, the crystal structure of ADA from *Plasmodium vivax* (*Pv*ADA) in a complex with MT-coformycin reveals an unprecedented binding geometry for 5′-methylthioribosyl groups in the malarial ADAs. Compared to malarial ADA complexes with adenosine or deoxycoformycin, 5′-methylthioribosyl groups are rotated 130°. A hydrogen bonding network between Asp172 and the 3′-hydroxyl of MT-coformycin is essential for recognition of the 5′-methylthioribosyl group. Water occupies the 5′-hydroxyl binding site when MT-coformycin is bound. Mutagenesis of Asp172 destroys the substrate specificity for MTA and MT-coformycin. Kinetic, mutagenic, and structural analyses of *Pv*ADA and kinetic analysis of five other *Plasmodium* ADAs establish the unique structural basis for its specificity for MTA and MT-coformycin. *Plasmodium gallinaceum* ADA does not use MTA as a substrate, is not inhibited by MT-coformycin, and is missing Asp172. Treatment of *P. falciparum* cultures with coformycin or MT-coformycin in the presence of MTA is effective in inhibiting parasite growth.

Malaria is caused by protozoan parasites of the *Plasmodium* genus. Within the four species of malaria parasite that infect humans, *Plasmodium vivax* and *Plasmodium falciparum* are the most prevalent species, with *P. falciparum* being responsible for most of the fatal cases (*1*). *P. vivax* has the widest global distribution and is responsible for most of the malaria cases in Central and South America and Asia (*2*). *Plasmodium knowlesi* is a primate malaria that is an emerging infectious disease of humans (*3*, *4*). Malaria treatment by chemotherapeutic and vector control strategies have not prevented its widespread occurrence. Recent increases in the resistance of malaria parasites to drug treatment and in mosquito vectors to insecticides have renewed the demand for new chemotherapeutic strategies (*5*, *6*). The 48 h intraerythrocytic parasite growth phase requires robust nucleic acid synthesis; thus, targeting of purine salvage pathways provides a promising route for novel drug development.

All *Plasmodium* species are purine auxotrophs, salvaging host cell purines for synthesis of cofactors and nucleic acids (*7*, *8*). In *Plasmodium*, adenosine is converted to hypoxanthine using adenosine deaminase (ADA)[1] and purine nucleoside phosphorylase (PNP). IMP is formed from hypoxanthine by hypoxanthine-guanine-xanthine phosphoribosyl transferase (HGXPRT). Inhibition of the purine salvage pathway with transition state analogue inhibitors of both human and *Plasmodium* PNP, such as Immucillin-H and 4′-deaza-1′-aza-2′-deoxy-1′-(9-methylene)-Immucillin-G (DADMe-ImmG), are lethal for *P. falciparum in vitro* (*9*, *10*).

Coformycin is a picomolar, transition state analogue inhibitor of both human and *Plasmodium* ADAs (*11*). Coformycin alone does not inhibit parasite growth in cultured erythrocytes (*10*), but

[†]This work was supported by National Institutes of Health (NIH) Grant AI049512, NIH Training Grants F31 AI05665 and CM007288, and U.S. Army Research Grant W81XWH-05-2-0025 and in part by a contract from the Medicines in Malaria (MMV) Consortium (Geneva, Switzerland).

[‡]Parts of this work were published in a thesis submitted by D.C.M. in partial fulfillment of the requirements for the Degree of Doctor of Philosophy in the Sue Golding Graduate Division of Medical Sciences, Albert Einstein College of Medicine, Yeshiva University.

*To whom correspondence should be addressed: Department of Biochemistry, Jack and Pearl Resnick Campus, 1300 Morris Park Ave., Bronx, NY 10461. Telephone: (718) 430-2813. Fax: (718) 430-8565. E-mail: vern@aecom.yu.edu.

[1]Abbreviations: ADA, adenosine deaminase; MTA, methylthioadenosine; MT-coformycin, methylthiocoformycin; PNP, purine nucleoside phosphorylase; HGXPRT, hypoxanthine-guanine-xanthine phosphoribosyl transferase; IMP, inosine 5′-monophosphate; MTI, methylthioinosine; d-coformycin, 2′-deoxycoformycin; Asp, aspartic acid; Glu, glutamic acid; His, histidine; Ala, alanine; Gly, glycine; Thr, threonine; Phe, phenylalanine; Met, methionine; Ile, isoleucine.

 Published on Web 09/03/2009

2′-deoxycoformycin (d-coformycin, Pentostatin) is reported to cause decreased parasitemia in *P. knowlesi*-infected primates (*12*). *Plasmodium* species lack adenosine kinase (*10*, *13*) and cannot incorporate exogenous adenosine directly into the adenylate pool. Thus, adenosine (or MTA) can only be salvaged after action of ADA in the parasite. Here, we demonstrate that *P. falciparum in vitro* growth is inhibited by coformycin or MT-coformycin with MTA as the purine source.

P. falciparum ADA (*Pf*ADA) also deaminates 5′-methylthioadenosine [MTA (Figure 1)] in addition to adenosine (*14*). Thus, *Pf*ADA serves the dual functions of adenosine salvage and recycling MTA formed from the synthesis of polyamines (*14*). Mammalian ADAs do not deaminate MTA and instead express a specific MTA phosphorylase for recycling of MTA (*14*). Mammalian erythrocytes do not synthesize polyamines. Thus, an intact polyamine synthetic pathway is important for the viability of malaria parasites (*14*, *15*). In *P. falciparum*, MTA is deaminated by *Pf*ADA to 5′-methylthioinosine (MTI), a metabolite that has not been reported in mammalian metabolism (*16*). The *Plasmodium* PNP also serves a dual purpose by converting both inosine and MTI to hypoxanthine for conversion to IMP and incorporation into nucleic acids (*14*).

We synthesized 5′-methylthiolcoformycin [MT-coformycin (Figure 1)] as a specific transition state analogue inhibitor of *Plasmodium* ADAs based on their unusual specificity for both adenosine and MTA (*11*). MT-Coformycin is a subnanomolar inhibitor of *Pf*ADA and demonstrates >20000-fold selectivity for *Pf*ADA relative to human ADA. This selectivity is remarkable since coformycin and d-coformycin are powerful picomolar inhibitors of both human and *P. falciparum* ADAs (*11*).

To understand the structural basis of recognition of *Pf*ADA for MTA and MT-coformycin, we overexpressed and characterized five additional ADAs from parasites with different host preferences: *P. vivax* (human), *P. knowlesi* (*P. falciparum*-like, simian host), *Plasmodium cynomolgi* (*P. vivax*-like, simian host), *Plasmodium berghei* (rodent host), and *Plasmodium gallinaceum* (avian host). Avian erythrocytes are nucleated, distinguishing them from mammalian red cells. Within the six *Plasmodium* ADAs tested, only *P. gallinaceum* ADA (*Pg*ADA) does not have significant activity for MTA, and consequently, MT-coformycin is a poor inhibitor. Sequence alignment revealed that *Pg*ADA differs in its catalytic site with an Asp172Glu replacement.

Recent crystal structures of *P. vivax* ADA (*Pv*ADA) revealed catalytic site interactions with adenosine and d-coformycin (*17*). Molecular modeling experiments hypothesized that the *Plasmodium* species enzymes can accommodate the 5′-methylthio substituent with only minor conformational changes to the catalytic site amino acids and to the ligand (*17*).

Here, we present the crystal structure of MT-coformycin bound to *Pv*ADA at 2.1 Å resolution. MT-Coformycin binds tightly as a consequence of a large change in the glycosidic torsion angle to reposition the 5′-methylthioribosyl group in a geometry previously unseen in other adenosine deaminase structures (*17*, *18*). The 1.9 Å resolution crystal structure and kinetic properties of a mutant lacking Asp172 (*Pv*ADA-ΔAsp172) established the mechanism of MT-coformycin binding.

EXPERIMENTAL PROCEDURES

Cloning and Expression of Adenosine Deaminase Enzymes from Different Plasmodium Species. Orthologs of *Pf*ADA were located using the tblastn function (default settings) with the *P. knowelsi*, *P. vivax*, *Plasmodium reichenowi*, *P. gallinaceum*, and *P. berghei* genome sequence databases from Sequencing Groups at the Sanger Institute (http://www.sanger.ac.uk/pathogens/malaria/), The Institute for Genomic Research Parasite Database (http://www.tigr.org/parasiteProjects.shtml), and PlasmoDB (http://plasmodb.org/). Appropriate primers were designed (Table S1 of the Supporting Information). *P. cynomolgi* ADA was cloned using degenerate primers based on the *P. reichenowi* sequence. In each strain, ADA was predicted to reside on a contiguous DNA sequence to permit cloning from genomic DNA. Genomic DNA from *P. berghei* (ANKA strain), *P. vivax* (Sal-1, gift of J. Carlton, New York University Langone Medical Center), *P. gallinaceum* (gift of J. Vinetz, University of California at San Diego School of Medicine), and *P. cynomolgi* and *P. knowlesi* (gift of C. Kocken and A. Thomas, Biomedical Primate Research Centre) was used for PCR amplification of the ADA gene from each species. The coding region of each enzyme, without the stop codon, was amplified by PCR and cloned into the pTrcHis2-TOPO vector (Invitrogen) with a C-terminal His_6 tag and ampicillin selection cassette. Each plasmid was transformed into *Escherichia coli* strain TOP10 (Invitrogen), and multiple clones of each DNA encoding ADA were sequenced and the data confirmed from the *P. knowlesi*, *P. vivax*, *P. gallinaceum*, and *P. berghei* genome predictions. The DNA sequence for *P. cynomolgi* ADA was determined and is reported as new data since no genome sequence data were available. The respective amino acid sequences of the malarial ADAs are reported (Figure S1 of the Supporting Information). The recombinant enzymes were expressed by induction of a 100 mL bacterial culture with 1 mM isopropyl 1-thio-β-D-galactopyranoside (IPTG) at 37 °C for 18 h and purified using nickel-nitrilotriacetic acid affinity chromatography (Ni-NTA spin column, Qiagen) according to the manufacturer's instructions. The purified proteins were used for enzymatic assays without further purification. Enzyme concentrations were determined from the extinction coefficients at 280 nm (Table S1 of the Supporting Information).

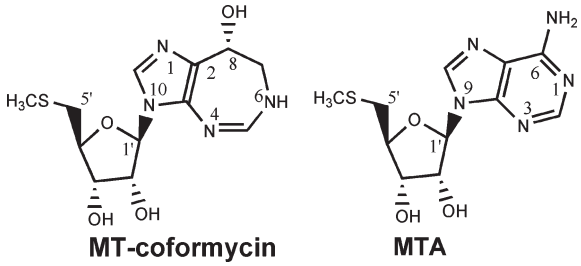

FIGURE 1: Structures and atomic numbering for MT-coformycin and methylthioadenosine (MTA).

P. falciparum in Vitro Cell Growth and Inhibition Assay. Coformycin and MT-coformycin were dissolved in water. Inhibition tests were conducted in flat-bottomed microtiter plates (Costar). The method described by Desjardins and colleagues (*19*) was used to determine the IC_{50} value, and the parasite DNA content was determined by DNA dye binding fluorescence as described by Quashie and colleagues (*20*). For each condition, three experiments were conducted in duplicate. Synchronized *P. falciparum* cultures were grown in purine-rich medium (370 μM hypoxanthine, standard medium). Prior to growth inhibition experiments, schizont stage parasite cultures were split, and one half was washed in purine-free medium and cultured in purine-free medium for 24 h while the other half was maintained in standard medium. Ring stage parasite cultures (200 μL per

well, with 1% hematocrit and 1% parasitemia) were grown for 72 h in the presence of increasing inhibitor concentrations in the presence of 100 μM MTA as the sole purine source. After incubation, cells were harvested and analyzed for DNA content. Uninfected erythrocytes were used as background controls.

Site-Directed Mutagenesis of P. vivax ADA. Site-directed mutagenesis used the QuickChange site-directed mutagenesis kit (Stratagene) according to the manufacturer's instructions. Appropriate primers were designed (Table S2 of the Supporting Information), and the mutagenesis reactions were performed using the pTcrHis2-TOPO vector containing the *Pv*ADA sequence as the template. The final reaction mixture was transformed into *E. coli* strain X10-Gold (Stratagene). Multiple clones of each ADA mutant were sequenced to confirm the presence of the desired mutation (Table S2 of the Supporting Information). The plasmids carrying the desired mutations were transformed into *E. coli* strain BL21-codon plus (DE3)-RIPL (Stratagene). The recombinant enzymes were expressed, purified, and quantified as described above.

Enzymatic Assays and Inhibition Studies. Recombinant proteins were used for enzymatic assays directly following purification. Adenosine deaminase activity was determined by monitoring the change in absorbance at 265 nm upon conversion of adenosine to inosine or MTA to MTI in 100 mM Tris-HCl buffer (pH 8.0) and varied concentrations of adenosine or MTA (*14*). Enzyme inhibition assays for determining the K_i value for initial and slow-onset inhibition constants (K_i*) were performed using different concentrations of coformycin or MT-coformycin and 200 μM adenosine. Inhibitors were synthesized and inhibition constants were determined as described previously (*11*).

Protein Purification and Crystallization. Recombinant *Pv*ADA and the mutant *Pv*ADA-ΔAsp172 were expressed by induction of the bacterial culture with 1 mM IPTG at 30 °C for 18 h. The cells were ruptured by being passed through a French press; the cell debris was removed by centrifugation, and the remaining supernatant was purified over a 3 mL Ni-NTA affinity column with elution by a step gradient of 10, 50, 75, 100, and 500 mM imidazole. Purified recombinant proteins were dialyzed overnight against 50 mM HEPES (pH 7.5), 50 mM NaCl, and 1 mM DTT. The final concentration of wild-type *Pv*ADA for crystallization was 10 mg/mL in the presence of 1 mM MT-coformycin. The crystallization condition [25% PEG3350, 100 mM Hepes (pH 7.5), and 0.2 M $MgCl_2$] was identified using Hampton Research Index HT screening by sitting-drop vapor diffusion. A condensed cluster of rod-shaped crystals was obtained. *Pv*ADA-ΔAsp172 (10 mg/mL) failed to cocrystallize with MT-coformycin but cocrystallized with 3 mM MTA in 0.2 M $MgCl_2$, 0.1 M BisTris (pH 5.5), and 25% PEG 3350. MTA was not present in the cocrystallized crystal (data not shown). These crystals were soaked with 2 mM MT-coformycin for 1 h to produce MT-coformycin bound to *Pv*ADA-ΔAsp172. Crystals were transferred into a fresh drop of the crystallization solution containing 20% glycerol and rapidly frozen in liquid nitrogen.

Data Collection and Processing. X-ray diffraction data of MT-coformycin bound to *Pv*ADA were collected at beamline 24-ID-E equipped with a MD-2 microdiffractometer at the Advanced Photo Source of Argonne National Laboratory (Argonne, IL). The microdiffractometer was used to search for a well-separated diffraction pattern among the crystal cluster. X-ray diffraction data of MT-coformycin-bound *Pv*ADA-ΔAsp172 were collected at beamline X29A at Brookhaven National Laboratory (Upton, NY). All data were processed with the HKL2000 program suite, and the data processing statistics are listed in Table 1 (*21*).

Table 1: X-ray Data Collection and Refinement Statistics

	*Pv*ADA in complex with MT-coformycin	*Pv*ADA-ΔAsp172 in complex with MT-coformycin
PDB entry	3EWC	3EWD
	Data Collection	
space group	$P2_12_12$	$P2_12_12_1$
cell dimensions		
a, *b*, *c* (Å)	87.0, 100.1, 43.6	41.9, 87.0, 106.1
α, *β*, *γ* (deg)	90, 90, 90	90, 90, 90
resolution (Å)	20−2.0 (2.03−2.00)[a]	20−1.9 (1.93−1.90)[a]
R_{merge} (%)	15.4 (67.8)[a]	9.7 (67.5)[a]
$I/\sigma I$	8.8 (1.4)[a]	14.8 (2.4)[a]
completeness (%)	99.1 (92.0)[a]	99.9 (100)[a]
redundancy	5.3 (2.7)[a]	2.9 (2.8)[a]
	Refinement	
resolution (Å)	20−2.1	20−1.9
no. of reflections ($F > 0\sigma F$)	21268	29669
R_{work} (%)/R_{free} (%)	20.4/25.4	20.3/24.8
B-factor (Å^2)		
Wilson *B*-factor	24	21
protein		
main chain	25	20
side chain	28	23
water	28	28
ligand	35	27
root-mean-square deviation from ideality (Å/deg)	0.014/1.49	0.018/1.73

[a]Numbers in parentheses show the statistics for the highest-resolution shell.

Structure Determination and Refinement. The crystal structure of *Pv*ADA bound to MT-coformycin was determined by molecular replacement in Molrep (*22*) using the published structure of *Pv*ADA bound to d-coformycin (PDB entry 2PGR) as the search model. The model without MT-coformycin and Zn^{2+} ion was first built in COOT (*23*) and refined in Refmac5. The Zn^{2+} ion was added and refined on the basis of the crystal studies by Larson and colleagues (*17*). The MT-coformycin was added last using the $F_o - F_c$ map and refined in Refmac5 (*24*). The crystal structure of *Pv*ADA-ΔAsp172 bound to MT-coformycin was determined in the same way as the crystal structure of *Pv*ADA bound to MT-coformycin. In both crystal structures, His253 and Asp310 coordinate the catalytic zinc ion and are the only residues whose torsion angles are in the disallowed region of the Ramachandron plot. The disfavored torsion angles of His254 and Asp310 are also observed and described in the three other published structures of *Pv*ADA with bound ligands (*17*). The final models were validated with Procheck in the absence of the disordered residues, including the first six amino acid residues and C-terminal linker with the His tag (*25*), and the refinement statistics are summarized in Table 1. The ligand-omit $mF_o - DF_c$ difference map and ligand-omit $2mF_o - DF_c$ electron density map, presented in Figures 4C and 5C, were calculated using phases from the final refined protein models from which the ligands were removed (*26*). Figures 3A and 4−7, where oxygen, nitrogen, and sulfur atoms are colored red, blue,

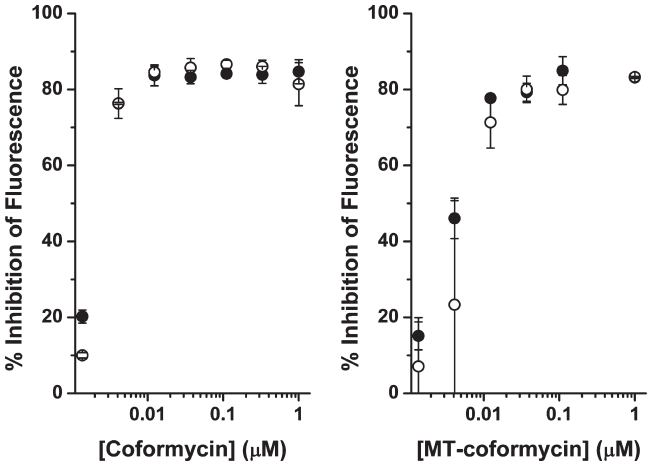

FIGURE 2: Inhibition of DNA synthesis in *P. falciparum* cultures treated with coformycin and MT-coformycin. Infected erythrocytes were cultured in the presence of 100 μM MTA in the presence of the indicated inhibitor concentrations for 72 h, followed by DNA analysis. Means and standard deviations are from three independent experiments: (○) culture incubated in purine-free medium prior to addition of the inhibitor and (●) cultures maintained in purine-rich medium until treatment. All treatments were performed in media containing MTA as the sole exogenous purine source.

and magenta, respectively, were created with Pymol (http://www.pymol.org).

RESULTS

Identification and Characterization of ADA from Various Plasmodium Species. Open reading frames for ADA from various *Plasmodium* species were identified and placed in expression vectors, and the expressed proteins were purified to characterize the kinetic parameters, substrate and inhibitor specificity. *P. falciparum* was used as a control since it had been previously characterized (*11*, *14*). The *Plasmodium* ADA amino acid sequences (Figure S1 of the Supporting Information) exhibit identity values ranging from 62 to 72% as compared to *Pf*ADA. The K_m values for adenosine ranged from 32 μM (*P. gallinaceum*) to 120 μM (*P. knowlesi*), while the K_m values for MTA varied from 4.4 μM (*P. berghei*) to 115 μM (*P. falciparum*) and had no detectable catalytic activity with *P. gallinaceum* ADA (Table 2). All ADAs had k_{cat}/K_m values near 10^4 M^{-1} s^{-1} with adenosine as the substrate. Similar values were obtained with MTA as the substrate with the exception of *Pg*ADA, which exhibited no detectable activity for MTA under conditions that would have detected 0.1% of that activity.

The K_i values for coformycin ranged from 2.3 nM (*P. berghei*) to 14 nM (*P. falciparum*), and the K_i* (slow-onset inhibition constant) varied from 0.25 nM (*P. berghei*) to 0.71 nM (*P. vivax*). Inhibition constants for MT-coformycin ranged from 3.2 nM (*P. falciparum*) to 48 nM (*P. knowlesi*) and showed no detectable inhibition with *P. gallinaceum*. Only *Pf*ADA and *Pb*ADA exhibited slow-onset inhibition for MT-coformycin, to give K_i* values of 0.25 and 5 nM, respectively (Table 3).

Effect of Coformycin and MT-Coformycin on P. falciparum DNA Biosynthesis. The effect of inhibiting parasite ADA or parasite and host ADAs was measured in the *P. falciparum* 3D7 strain cultured in human erythrocytes. DNA content was analyzed following treatment with coformycin (inhibitor of both human and parasite ADAs) or MT-coformycin (inhibitor of parasite ADA) for 72 h in the presence of MTA. The

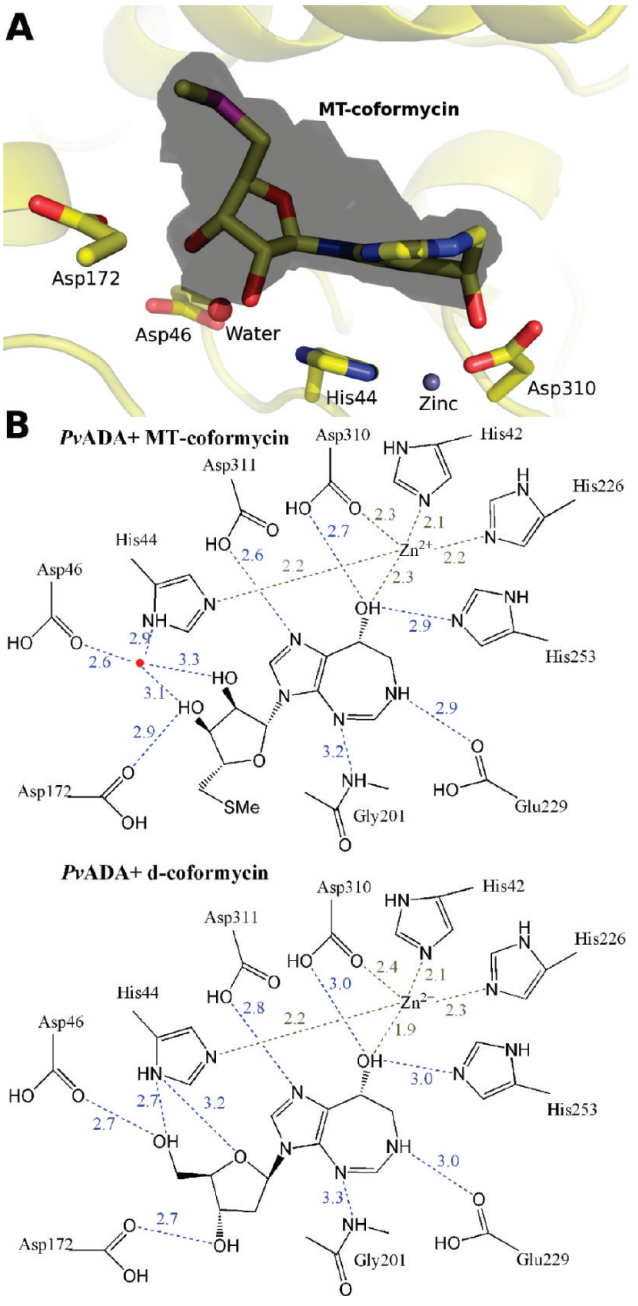

FIGURE 3: (A) Solvent accessible surface map of a cut-surface diagram of *Pv*ADA with bound MT-coformycin. The solvent accessible map (colored gray) shows an enclosed cavity comprising the active site of *Pv*ADA. The 5′-methylthiol group of MT-coformycin (shown in the surface map) fits tightly into this cavity. The side chains of Asp172, His42, and Asp45 and a structural water are shown. The water molecule replaces the 5′-hydroxyl group of adenosine when 5′-methylthioribosyl groups are bound. The side chain of Asp172 is in hydrogen-bond contact with the 3′-hydroxyl group. (B) Relative position of MT-coformycin (this study) compared to d-coformycin (PDB entry 2PGR) and the active site residues of *Pv*ADA. The water molecule is drawn as a red dot. The hydrogen bonds and zinc ion interactions are depicted as blue and gray dashed lines (angstroms), respectively.

inhibitors reduced the level of parasite DNA synthesis with IC_{50} values of 2 nM for coformycin and 5 nM for MT-coformycin when 100 μM MTA was provided as the exogenous purine source (Figure 2). Adenosine and MTI were also tested as exogenous purine sources, but no inhibition was detected (data not shown).

Characterization of PvADA Mutants. On the basis of the crystal structure of *Pv*ADA with bound MT-coformycin

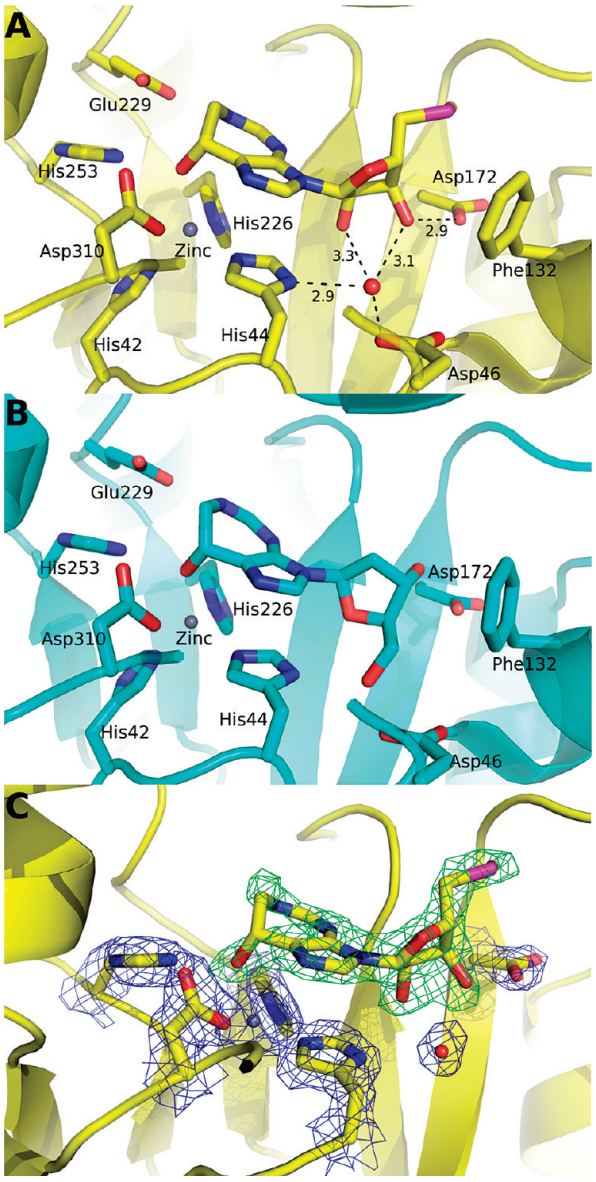

FIGURE 4: Comparative geometry of MT-coformycin and d-coformycin in the active site of *Pv*ADA. (A) MT-Coformycin in the catalytic site of *Pv*ADA is colored yellow. The hydrogen bonds between the ribosyl group of MT-coformycin and adjacent catalytic site molecules are shown as dashed lines, and distances are given in angstroms. The Zn^{2+} ion is colored gray. (B) Positions of d-coformycin bound to *Pv*ADA colored blue and Zn^{2+} ion gray. (C) Ligand-omit electron density map of MT-coformycin-bound *Pv*ADA. The MT-coformycin-omit $mF_o - DF_c$ difference map is colored green at a contour level of 3.0σ, and the MT-coformycin-omit $2mF_o - DF_c$ electron density map of His44, His226, His253, Asp172, Asp310, and a structural water is colored blue at a contour level of 1.4σ.

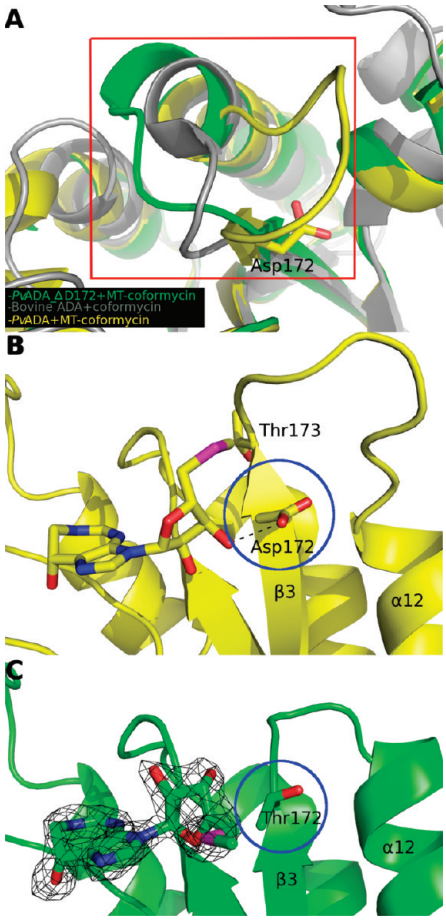

FIGURE 5: Asp172−Ile180 region of ADA structures consisting of *Pv*ADA with MT-coformycin, bovine ADA with 6-hydroxy-1, 6-dihydropurine riboside, and *Pv*ADA-ΔAsp172 with MT-coformycin. (A) Inhibitor-bound ADAs are depicted as ribbon diagrams and colored yellow (*Pv*ADA), gray (bovine ADA, PDB entry 1KRM), and green (*Pv*ADA-ΔAsp172). To indicate the position of the active site, Asp172 of MT-coformycin-bound *Pv*ADA is shown. The *Plasmodium*-specific Asp172−Ile180 region from *Pv*ADA is enclosed in the red box. The *Plasmodium*-specific region of inhibitor-bound *Pv*ADA-ΔAsp172 bears greater structural resemblance to the equivalent region of inhibitor-bound bovine ADA than to *Pv*ADA. (B) Expanded view of the *Plasmodium*-specific region of MT-coformycin-bound *Pv*ADA. The hydrogen bonding interaction between Asp172 and *Pv*ADA-bound MT-coformycin is represented by a dashed line. (C) Expanded view of the *Plasmodium*-specific region of MT-coformycin-bound *Pv*ADA-ΔAsp172. The MT-coformycin-omit $mF_o - DF_c$ difference map is colored black at a contour level of 3.0σ. MT-Coformycin and the side chains of Asp172, Thr173, and Ile180 are depicted as stick models. The deletion of Asp172 results in a reorganization of the *Plasmodium*-specific region in *Pv*ADA-ΔAsp172 that includes shortening of strand β3 and elongation of helix α12.

(see below), three *Pv*ADA mutants were designed (Table S2 of the Supporting Information) to test the importance of Asp172 in methylthio-group recognition. Kinetic constants were determined under the same conditions as for wild-type *Pv*ADA (Table 4). All Asp172 mutants lost the ability to deaminate MTA and lost their high affinity for MT-coformycin. *Pv*ADA-Glu172 exhibited weak catalytic activity at elevated enzyme concentrations (data not shown). In contrast to the loss of 5′-methylthio group specificity, the deletion of Asp172 produced only a small effect on the catalytic efficiency for adenosine and the binding of coformycin.

Structure of PvADA with MT-Coformycin. The structure of *Pv*ADA in complex with MT-coformycin was determined and refined to a final resolution of 2.1 Å. *Pv*ADA is a typical TIM barrel, composed of eight α-helices and eight β-strands with 16 α-helices of accessory structure. With MT-coformycin bound in the active site, the Asp172−Ile180 region (part of the β3 strand and β3−α12 loop) shifts approximately 15 Å compared to the open structure reported for apo *Plasmodium yoelli* ADA (*17*). This movement forms a closed foot-shaped cavity in the active site with the 2′- and 3′-hydroxyl groups of the MT-coformycin in the heel portion of the foot-shaped cavity (Figure 3A).

Geometry of MT-Coformycin in PvADA. The 8-(*R*)-hydroxydiazepine ring of MT-coformycin mimics the 6-(*R*)-hydroxyl tetrahedral Meisenheimer intermediate, similar to the

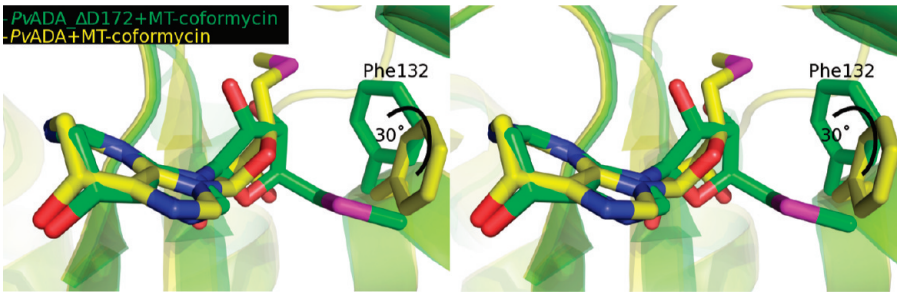

FIGURE 6: Stereoview of overlaid structures of MT-coformycin bound to *Pv*ADA or *Pv*ADA-ΔAsp172. The MT-coformycin and *Pv*ADA are colored yellow, while MT-coformycin in the geometry bound to *Pv*ADA-ΔAsp172 is colored green. Phe132 rotates approximately 30° to accommodate the methylthio group.

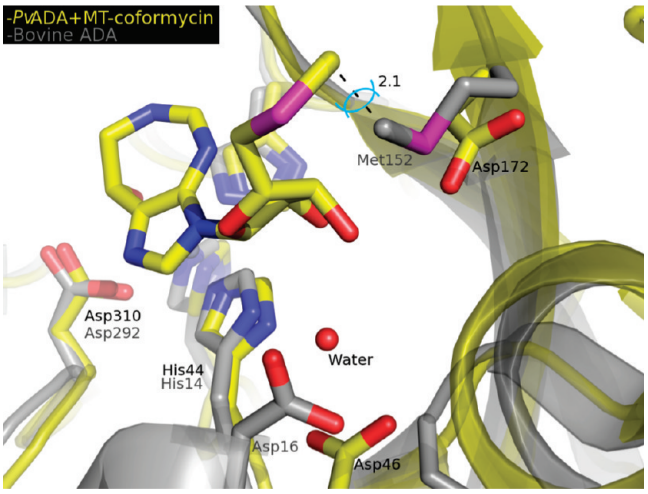

FIGURE 7: Overlaid catalytic site residues from *Pv*ADA with bound MT-coformycin are compared to bovine ADA with bound 6-hydroxy-1,6-dihydropurine riboside. Only the MT-coformycin ligand is shown (colored yellow). Residues from bovine ADA (PDB entry 1KRM) are colored gray. The van der Waals overlap between the methylthiol group from MT-coformycin and the Met at the catalytic site of bovine ADA is shown to be 2.1 Å. The residues of *Pv*ADA and bovine ADA are labeled in yellow and gray, respectively.

transition state formed by the attack of water at C6 of adenosine. The 8-(*R*)-hydroxy group of MT-coformycin replaces the attacking water nucleophile and is chemically stable since the position normally occupied by the leaving group amine in the adenosine transition state is replaced with a hydrogen. This hydrogen is facing the solvent, consistent with solvent water acting as the donor of the proton to NH_2 to form the NH_3 leaving group. The diazepine ring is positioned near the toe of a foot-shaped cavity (Figure 3), where in addition to the zinc ion interactions, N1H of the ring donates a hydrogen bond to Glu229. This is a specific transition state interaction since in the normal reaction N1 of adenosine is a H-bond acceptor while at the transition state it is rehybridized to N1H to become a H-bond donor, as in the bound MT-coformycin. His253, Asp310, and Asp311 and the backbone of Gly201 interact with MT-coformycin in a manner similar to that of the interactions with adenosine, the normal substrate (Figure 4A,C).

The 5′-methylthio group is displaced from the 5′-hydroxyl group binding site and is replaced with a structurally defined water molecule held in place by hydrogen bonds with His44, Asp46, and the 2′- and 3′-hydroxyl groups of MT-coformycin (Figures 3A and 4A). The 3′-hydroxyl group of MT-coformycin also forms a hydrogen bond with Asp172. This geometry of hydrogen bonds requires a 130° rotation of the ribosyl group around the glycosyl torsion angle (Table 5) with respect to bound adenosine (*17*). The position of the 5′-methylthio group (Figure 4A,B) causes it to be positioned almost 180° relative to the 5′-hydroxyl group found with bound adenosine, guanosine, and d-coformycin (*17*). Despite the dramatic alteration of the MT-ribose group geometry with respect to bound ribosyl groups, only a slight shift of the diazepine ring (approximately 0.4 Å) occurs relative to the position of d-coformycin in the active site (Figure 4A,B). These changes place the 5′-methylthio group near the ankle region of the foot-shaped cavity, directed toward the protein surface (Figure 3A). The 5′-methylthio group fits closely into a hydrophobic cavity without room for crystallographically ordered water molecules. The geometry of bound MT-coformycin provides a sharp contrast to adenosine, guanosine, and d-coformycin, where the 5′-hydroxyl group forms hydrogen bonds with His44 and Asp46 and points toward the protein core (Figure 4A,B).

MT-Coformycin in the Active Site of PvADA-ΔAsp172. On the basis of the structural comparison between bovine ADA with bound 6-hydroxy-1,6-dihydropurine riboside (Figure 5A, structure colored gray) and *Pv*ADA with MT-coformycin bound (Figure 5B, structure colored yellow) and the primary sequence alignment between mammalian and *Plasmodium* ADAs (Figure S1 of the Supporting Information), we hypothesized that an extra amino acid insertion into *Pv*ADA is responsible for the observed conformational differences between mammalian and *Plasmodium* ADAs. We deleted Asp172 of *Pv*ADA to shift Thr173 to the Thr172 position (Figure 5B,C). In mammalian ADAs, a Met is present at the equivalent position. The crystal structure of *Pv*ADA-ΔAsp172 in complex with MT-coformycin shows an open Asp172−Ile180 region (Figure 5A, structure colored green), similar to bovine ADA in complex with the inhibitor (Figure 5A, structure colored gray). In *Pv*ADA-ΔAsp172, with Thr172 now replacing the Asp group, the hydrogen bond with the 3′-hydroxyl group of MT-coformycin is lost (Figure 5B,C). In *Pv*ADA-ΔAsp172, the ribosyl group of MT-coformycin rotates to the orientation found for d-coformycin in *Pv*ADA (Figure 6). Phe132, located near His44 and Asp46, swings 30° away from the active site to accommodate the 5′-methylthio group (Figure 6). The unfavorable nature of this geometry for 5′-methylthioribose group binding is apparent in a 200-fold decrease in affinity for MT-coformycin (Table 4). The relative energetic contributions from methylthio and ribosyl group interactions are not available from these structures but cause an energy loss of ~3 kcal/mol.

DISCUSSION

Function of Plasmodium and Mammalian ADAs. Malarial parasites express relatively large quantities of ADA protein,

Table 2: Kinetic Constants for *Plasmodium* ADAs with Adenosine and 5′-Methylthioadenosine (MTA) as Substrates

	adenosine			MTA		
species	K_m (μM)	k_{cat} (s^{-1})	k_{cat}/K_m (M^{-1} s^{-1})	K_m (μM)	k_{cat} (s^{-1})	k_{cat}/K_m (M^{-1} s^{-1})
P. vivax	60 ± 6	1.8	3.0×10^4	9.5 ± 0.8	0.13	1.4×10^4
P. falciparum	88 ± 4	5.6	6.4×10^4	115 ± 14	5.8	5.0×10^4
P. cynomolgi	87 ± 9	5.3	6.1×10^4	8.7 ± 0.5	0.31	3.6×10^4
P. knowlesi	120 ± 12	6.8	5.7×10^4	22 ± 3	0.51	2.3×10^4
P. berghei	57 ± 2	4.7	8.2×10^4	4.4 ± 0.6	0.35	7.9×10^4
P. gallinaceum	32 ± 5	1.9	5.9×10^4	not detected	not detected	not detected

suggesting its metabolic importance in the essential purine salvage pathway. Coformycin (*10*) and d-coformycin (*27*) are weak inhibitors of parasite growth in cultured erythrocytes, but d-coformycin has been reported to decrease the parasitemia in primates infected with *P. knowlesi* (*12*). The action of ADA inhibitors *in vivo* suggests ADA as a potential target for antimalarials. ADA from *P. falciparum* also functions to deaminate MTA, a byproduct of polyamine synthesis. In *Plasmodium*, ADA converts MTA to MTI and purine nucleoside phosphorylase converts MTI to hypoxanthine and 5-methylthio-α-D-ribose 1-phosphate. These enzymes form the only known pathway for MTA catabolism in *Plasmodium*, a necessary step for MTA recycling to methionine and *S*-adenosylmethionine. Human ADA has not evolved for MTA deamination activity since methylthioadenosine phosphorylase (MTAP) and adenine phosphoribosyltransferase recycle the purine base in humans (*28*). Neither of these enzymes is encoded in the *P. falciparum* genome (*13*). We tested the effect of coformycin and MT-coformycin in *P. falciparum* cultures in the presence of 100 μM MTA as an exogenous purine source (Figure 2). Under these conditions, coformycin and MT-coformycin reduce the level of DNA synthesis of *P. falciparum in vitro* by approximately 80%, supporting *Plasmodium* ADA as the pathway for MTA metabolism. Equivalent inhibition of DNA synthesis by coformycin and MT-coformycin establishes the parasite ADA as the target since coformycin is a picomolar inhibitor of host and parasite ADAs while MT-coformycin inhibits only the *Plasmodium* ADA. Use of MT-coformycin as a potential antimalarial avoids the neurotoxicity of ADA inhibitors (such as Pentostatin and d-coformycin) in humans (*29*).

Species Specificity for MT-Coformycin Action. Other *Plasmodium* species were examined for the substrate specificity of their ADAs. *Plasmodium* species that infect mammals (*P. vivax*, *P. berghei*, *P. knowlesi*, and *P. cynomolgi*) exhibited robust catalytic efficiency for both adenosine and MTA. In contrast, *P. gallinaceum* infects bird erythrocytes and its ADA had no significant catalytic ability with MTA and was not inhibited by MT-coformycin (Tables 2 and 3). Avian erythrocytes differ from those in mammals in that they are nucleated, larger in size, and oblate ellipsoid in shape. The presence of nucleus, ribosomes, Golgi, and mitochondria creates a different metabolic environment for the malaria parasite, as purines and polyamines can be salvaged or synthesized *de novo* in avian erythrocytes (*30*). The ADA specificity of *P. gallinaceum* suggests that activity for MTA deamination is unnecessary in this parasite as no MTA would be formed within the parasites if polyamines are salvaged from the host. This species difference provides a convenient tool for exploring the catalytic site elements involved in 5′-methylthio group recognition. As shown below, the replacement of Asp172 with Glu172 in *P. gallinaceum* is important in its restricted activity for 5′-methylthioribosyl groups.

Table 3: Inhibition Constants of Transition State Analogue Inhibitors for *Plasmodium* ADAs

	coformycin		MT-coformycin	
species	K_i[a] (nM)	K_i*[b] (nM)	K_i[a] (nM)	K_i*[b] (nM)
P. vivax	7.4 ± 0.8	0.71 ± 0.09	20 ± 5	not detected
P. falciparum	14 ± 3	0.26 ± 0.03	3.2 ± 0.6	0.25 ± 0.05
P. knowlesi	3.4 ± 0.7	0.64 ± 0.04	48 ± 7	not detected
P. cynomolgi	7 ± 2	0.41 ± 0.04	30 ± 3	not detected
P. berghei	2.3 ± 0.4	0.15 ± 0.01	14 ± 3	5.0 ± 1.2
P. gallinaceum	4.7 ± 0.7	0.5 ± 0.1	29000 ± 6000	not detected

[a] K_i is the dissociation constant for the inhibitor during initial rate kinetic measurements. [b] K_i* is the dissociation constant for the inhibitor following a slow-onset tight-binding phase of inhibition.

ADA Catalytic Site Determinants for MTA Recognition. On the basis of the crystal structures, sequence alignment, and mutagenesis (see below), Asp172 is essential for the methylthio specificity (Table 4). The crystal structure of MT-coformycin bound to *Pv*ADA established a remarkable spatial rearrangement of methylthio derivatives. Although most *Plasmodium* ADAs bind both coformycin and MT-coformycin with picomolar affinity, the orientation of the 5′-methylthioribosyl group of MT-coformycin is altered relative to d-coformycin. In nucleosides and d-coformycin, the 5′-hydroxyl group is H-bonded to His44 and Asp46. The 5′-methylthio group is not accommodated in the 5′-hydroxyl binding site, and the ribose is rotated by 130° to permit the 3′-hydroxyl group to hydrogen bond to Asp172. The 5′-hydroxyl group is replaced with a water molecule, and the 5′-methylthio group relocates to a more hydrophobic region of the catalytic site, near Phe132 (Figure 6). This rotation and the interaction of Asp172 with the 3′-hydroxyl group are critical to permit MT-coformycin and MTA binding. In *Plasmodium* ADAs, an Asp172 signature at the 5′-binding site indicates the ability of ADAs to accept MTA as a substrate and to be inhibited by tight binding of MT-coformycin. In mammalian ADAs, Met152 occupies the position equivalent to *Pv*ADA-ΔAsp172. Met152 prevents binding of 5′-methylthio derivatives because of a spatial clash, and this region of the sequence is completely conserved in mouse, bovine, and human ADAs (Figure 7).

Substrate and Inhibitor Interactions in Plasmodium ADAs. Of the six species of *Plasmodium* ADAs examined here, only *P. gallinaceum*, in which Asp172 is replaced with Glu, is catalytically inactive with MTA. Mutated *Pv*ADAs (Asp172Ala, Asp172Glu, and ΔAsp172) exhibit catalytic characteristics similar to those of *P. gallinaceum* ADA. The hydrogen bond between the 3′-hydroxyl group of methylthio derivatives and Asp172 is

Table 4: Kinetic and Inhibition Constants for *Pv*ADA Mutants

	adenosine			coformycin	
	K_m (μM)	k_{cat} (s^{-1})	k_{cat}/K_m (M^{-1} s^{-1})	K_i (nM)	K_i* (nM)
P. vivax (wild type)	60 ± 6	1.8	3.0×10^4	7.4 ± 0.8	0.71 ± 0.09
*Pv*ADA-ΔAsp172	43 ± 5	2.8	6.5×10^4	7.3 ± 0.9	0.60 ± 0.08
*Pv*ADA-Ala172	104 ± 16	14.0	1.3×10^5	1.8 ± 0.5	1.0 ± 0.3
*Pv*ADA-Glu172	83 ± 15	12.9	1.5×10^5	1.5 ± 0.3	0.5 ± 0.1
	MTA			MT-coformycin	
	K_m (μM)	k_{cat} (s^{-1})	k_{cat}/K_m (M^{-1} s^{-1})	K_i (nM)	K_i* (nM)
P. vivax (wild type)	9.5 ± 0.8	0.13	1.4×10^4	20 ± 5	not detected
*Pv*ADA-ΔAsp172	not detected	not detected	not detected	4100 ± 1500	not detected
*Pv*ADA-Ala172	not detected	not detected	not detected	not detected	not detected
*Pv*ADA-Glu172	not detected	not detected	not detected	> 5000	not detected

Table 5: Glycosyl Torsion Angles

	dihedral angle (O4′−C1′−N9−C4 or O4′−C1′−N10−C3) (deg)	PDB entry
*Pv*ADA in complex with adenosine	−121.2	2PGF
*Pv*ADA in complex with d-coformycin	−122.4	2PGR
*Pv*ADA in complex with MT-coformycin	107.3	3EWC
*Pv*ADA-ΔAsp172 in complex with MT-coformycin	−144.7	3EWD

required to permit methylthio derivative binding and thereby assist in anchoring the purine or diazepine rings. Critically, this geometric change in the methylthioribose occurs while the purine group is still permitted to achieve alignment with the catalytic site Zn^{2+} as needed for activation of the water nucleophile at the reaction center. Without the hydrogen bond between the 3′-hydroxyl group and Asp172, the methylthioribosyl group adopts the ribosyl conformation found in adenosine and d-coformycin binding. In that case, the methylthio group is unfavorably positioned in the hydrophilic pocket near Asp46, His44, and a crystallographic water site. Kinetic evidence of this ribosyl conformational shift comes from the 200-fold weaker inhibition of MT-coformycin for *Pv*ADA-ΔAsp172 than for *Pv*ADA. Likewise, the *P. gallinaceum* ADA, containing Asp172Glu, binds MT-coformycin 14500-fold weaker than *Pv*ADA.

CONCLUSION

Plasmodium ADAs capable of using adenosine and MT-adenosine do so by accommodating the 5′-ribosyl and 5′-methylthioribosyl groups, respectively, in different geometries. The 5′-ribosyl groups of substrates and inhibitors form hydrogen bonds with His44 and Asn46 in a 5′-hydroxyl group site. The 5′-methylthioribosyl substrates and inhibitors bind with the ribosyl groups in a different geometry with a hydrogen bond between the 3′-hydroxyl and Asp172. Mutation of Asp172 eliminates efficient deamination of MTA and MT-coformycin binding. A critical feature of this unusual geometrically linked specificity in ADA is the ability to rotate the ribose groups of methylthioribosyl derivatives in the active site of *Plasmodium* ADAs while maintaining the register of the catalytic site elements with the site of hydrolytic deamination. Humans use MTAP to convert MTA to adenine and 5-methylthioribose 1-phosphate by phosphorolysis, and human ADA does not deaminate MTA. *Plasmodium* species have no MTAP, and most species deal with MTA by deamination using the double-specificity ADAs featuring Asp172 as an essential catalytic site specificity element. A replacement of Asp172 on ADAs by intentional mutation causes loss of MTA deaminase activity and MT-coformycin binding. The absence of Asp172 in the case of *P. gallinaceum* has the same effect. Catalytic site flexibility in the malarial ADAs permits efficient purine metabolism with fewer expressed proteins.

ACKNOWLEDGMENT

X-ray diffraction data for this study were measured at beamline X29A of the National Synchrotron Light Source and beamline 24-ID-E at the Northeastern Collaborative Access Team Beamlines of the Advanced Photon Source. Financial support of Beamline X29A comes principally from the Offices of Biological and Environmental Research and of Basic Energy Sciences of the U.S. Department of Energy, and from the National Center for Research Resources of the NIH. The Northeastern Collaborative Access Team beamline of the Advanced Photon Source is supported by Grant RR-15301 from the National Center for Research Resources at the NIH. Use of the Advanced Photon Source is supported by the U.S. Department of Energy, Office of Basic Energy Sciences, under Contract DE-AC02-06CH11357.

SUPPORTING INFORMATION AVAILABLE

Primer sequences used for cloning of adenosine deaminase from different *Plasmodium* species and primer sequences used for site-directed mutagenesis of *Pv*ADA and sequence alignment of *Plasmodium* and mammalian ADAs. This material is available free of charge via the Internet at http://pubs.acs.org.

REFERENCES

1. Snow, R. W., Guerra, C. A., Noor, A. M., Myint, H. Y., and Hay, S. I. (2005) The global distribution of clinical episodes of *Plasmodium falciparum* malaria. *Nature 434*, 214–217.
2. Mendis, K., Sina, B. J., Marchesini, P., and Carter, R. (2001) The neglected burden of *Plasmodium vivax* malaria. *Am. J. Trop. Med. Hyg. 64*, 97–106.
3. Jongwutiwes, S., Putaporntip, C., Iwasaki, T., Sata, T., and Kanbara, H. (2004) Naturally acquired *Plasmodium knowlesi* malaria in human, Thailand. *Emerging Infect. Dis. 10*, 2211–2213.

4. Cox-Singh, J., Davis, T. M., Lee, K. S., Shamsul, S. S., Matusop, A., Ratnam, S., Rahman, H. A., Conway, D. J., and Singh, B. (2008) *Plasmodium knowlesi* malaria in humans is widely distributed and potentially life threatening. *Clin. Infect. Dis. 46*, 165–171.
5. Hyde, J. E. (2005) Drug-resistant malaria. *Trends Parasitol. 21*, 494–498.
6. Hyde, J. E. (2007) Drug-resistant malaria: An insight. *FEBS J. 274*, 4688–4698.
7. de Koning, H. P., Bridges, D. J., and Burchmore, R. J. (2005) Purine and pyrimidine transport in pathogenic protozoa: From biology to therapy. *FEMS Microbiol. Rev. 29*, 987–1020.
8. Hyde, J. E. (2007) Targeting purine and pyrimidine metabolism in human apicomplexan parasites. *Curr. Drug Targets 8*, 31–47.
9. Kicska, G. A., Tyler, P. C., Evans, G. B., Furneaux, R. H., Schramm, V. L., and Kim, K. (2002) Purine-less death in *Plasmodium falciparum* induced by immucillin-H, a transition state analogue of purine nucleoside phosphorylase. *J. Biol. Chem. 277*, 3226–3231.
10. Cassera, M. B., Hazleton, K. Z., Riegelhaupt, P. M., Merino, E. F., Luo, M., Akabas, M. H., and Schramm, V. L. (2008) Erythrocytic adenosine monophosphate as an alternative purine source in *Plasmodium falciparum*. *J. Biol. Chem. 283*, 32889–32899.
11. Tyler, P. C., Taylor, E. A., Frohlich, R. F., and Schramm, V. L. (2007) Synthesis of 5′-methylthio coformycins: Specific inhibitors for malarial adenosine deaminase. *J. Am. Chem. Soc. 129*, 6872–6879.
12. Webster, H. K., Wiesmann, W. P., and Pavia, C. S. (1984) Adenosine deaminase in malaria infection: Effect of 2'-deoxycoformycin *in vivo*. *Adv. Exp. Med. Biol. 165* (Part A), 225–229.
13. Gardner, M. J., Hall, N., Fung, E., White, O., Berriman, M., Hyman, R. W., Carlton, J. M., Pain, A., Nelson, K. E., Bowman, S., Paulsen, I. T., James, K., Eisen, J. A., Rutherford, K., Salzberg, S. L., Craig, A., Kyes, S., Chan, M. S., Nene, V., Shallom, S. J., Suh, B., Peterson, J., Angiuoli, S., Pertea, M., Allen, J., Selengut, J., Haft, D., Mather, M. W., Vaidya, A. B., Martin, D. M., Fairlamb, A. H., Fraunholz, M. J., Roos, D. S., Ralph, S. A., McFadden, G. I., Cummings, L. M., Subramanian, G. M., Mungall, C., Venter, J. C., Carucci, D. J., Hoffman, S. L., Newbold, C., Davis, R. W., Fraser, C. M., and Barrell, B. (2002) Genome sequence of the human malaria parasite *Plasmodium falciparum*. *Nature 419*, 498–511.
14. Ting, L. M., Shi, W., Lewandowicz, A., Singh, V., Mwakingwe, A., Birck, M. R., Ringia, E. A., Bench, G., Madrid, D. C., Tyler, P. C., Evans, G. B., Furneaux, R. H., Schramm, V. L., and Kim, K. (2005) Targeting a novel *Plasmodium falciparum* purine recycling pathway with specific immucillins. *J. Biol. Chem. 280*, 9547–9554.
15. Trackman, P. C., and Abeles, R. H. (1983) Methionine synthesis from 5′-S-methylthioadenosine. Resolution of enzyme activities and identification of 1-phospho-5-S-methylthioribulose. *J. Biol. Chem. 258*, 6717–6720.
16. Olszewski, K. L., Morrisey, J. M., Wilinski, D., Burns, J. M., Vaidya, A. B., Rabinowitz, J. D., and Llinas, M. (2009) Host-parasite interactions revealed by *Plasmodium falciparum* metabolomics. *Cell Host Microbe 5*, 191–199.
17. Larson, E. T., Deng, W., Krumm, B. E., Napuli, A., Mueller, N., Van Voorhis, W. C., Buckner, F. S., Fan, E., Lauricella, A., DeTitta, G., Luft, J., Zucker, F., Hol, W. G., Verlinde, C. L., and Merritt, E. A. (2008) Structures of substrate- and inhibitor-bound adenosine deaminase from a human malaria parasite show a dramatic conformational change and shed light on drug selectivity. *J. Mol. Biol. 381*, 975–988.
18. Wang, Z., and Quiocho, F. A. (1998) Complexes of adenosine deaminase with two potent inhibitors: X-ray structures in four independent molecules at pH of maximum activity. *Biochemistry 37*, 8314–8324.
19. Desjardins, R. E., Canfield, C. J., Haynes, J. D., and Chulay, J. D. (1979) Quantitative assessment of antimalarial activity *in vitro* by a semiautomated microdilution technique. *Antimicrob. Agents Chemother. 16*, 710–718.
20. Quashie, N. B., de Koning, H. P., and Ranford-Cartwright, L. C. (2006) An improved and highly sensitive microfluorimetric method for assessing susceptibility of *Plasmodium falciparum* to antimalarial drugs *in vitro*. *Malar. J. 5*, 95.
21. Otwinowski, Z., and Minor, W. (1997) Processing of X-ray Diffraction Data Collected in Oscillation Mode. *Methods Enzymol. 276*, 307–326.
22. Vagin, A. A., and Teplyakov, A. (1997) MOLREP: An Automated Program for Molecular Replacement. *J. Appl. Crystallogr. 30*, 1022–1025.
23. Emsley, P., and Cowtan, K. (2004) Coot: Model-building tools for molecular graphics. *Acta Crystallogr. D60*, 2126–2132.
24. Murshudov, G. N., Vagin, A. A., and Dodson, E. J. (1997) Refinement of macromolecular structures by the maximum-likelihood method. *Acta Crystallogr. D53*, 240–255.
25. Laskowski, R. A., McArthur, M. W., Moss, D. S., and Thornton, J. M. (1993) PROCHECK: A program to check the stereochemical quality of protein structures. *J. Appl. Crystallogr. 265*, 283–291.
26. Read, R. J. (1986) Improved Fourier coefficients for maps using phases from partial structures with errors. *Acta Crystallogr. A42*, 140–149.
27. Roth, E. Jr., Ogasawara, N., and Schulman, S. (1989) The deamination of adenosine and adenosine monophosphate in *Plasmodium falciparum*-infected human erythrocytes: *In vitro* use of 2′-deoxycoformycin and AMP deaminase-deficient red cells. *Blood 74*, 1121–1125.
28. Singh, V., and Schramm, V. L. (2006) Transition-state structure of human 5′-methylthioadenosine phosphorylase. *J. Am. Chem. Soc. 128*, 14691–14696.
29. Sauter, C., Lamanna, N., and Weiss, M. A. (2008) Pentostatin in chronic lymphocytic leukemia. *Expert Opin. Drug Metab. Toxicol. 4*, 1217–1222.
30. Stevens, L. (1996) Avian Biochemistry and Molecular Biology, Cambridge University Press, New York.